Betatron motion and linear undulator brightness: Inhomogeneous broadening effects due to electron-beam emittance and Twiss parameters

G. Dattoli, G. K. Voykov, and M. Carpanese
Ente Perlenuove Technologie, L'Energia e L'ambiente, Dipartimento Innovazione, Settore Fisica Applicata, Centro Ricerche Frascati, P.O. Box 65, 00044 Frascati, Rome, Italy
(Received 3 October 1994; revised manuscript received 6 July 1995)

The combined effects of electron-beam betatron motion and non-negligible emittance provide a rich phenomenology of the radiation emitted in linearly polarized undulators. Indeed, even harmonics may be radiated on axis and the induced inhomogeneous broadenings depend on the electron-beam matching condition. We discuss the dependence of undulator brightness on electron-beam betatron motion and also analyze how the harmonic spectrum depends on the electron-beam emittance and Twiss parameters. We present independent analytical and numerical analyses, make a comparison between the two methods, and comment on the limits of the analytical treatment.

PACS number(s): 41.60.Cr, 41.85.Lc, 52.75.Ms, 07.77.−n

I. INTRODUCTION

The influence of betatron motion on undulator brightness has been recently accounted for, and the combined effects of beam emittances and Twiss coefficients on the broadening of the undulator radiation spectrum have been discussed [1]. The results of the analysis can be summarized as follows: (1) Line broadening depends on the electron-beam Twiss parameters and emittances. (2) Deviations from the matching condition provide further line broadening and peak brightness reduction. (3) The harmonic content of the emitted radiation is much richer.

In this paper we will reconsider the above problems within the context of a numerical treatment. Before entering into specific details, we should make some preliminary points: (a) We consider the case of linear undulator brightness, which is calculated including the transverse components of the magnetic field whose on-axis component is assumed to be polarized along the y direction. (b) The undulator is focusing equally along the vertical components of the electron motion and the associated betatron frequencies are [1]

$$\Omega_x=\Omega_y=\frac{1}{2}\frac{K}{\gamma}\Omega_u \ , \tag{1}$$

where B_0 is the peak on-axis magnetic field, λ_u is the undulator period, N is the number of undulator periods, $L_u=N\lambda_u$ is the length of the undulator, $K=eB_0\lambda_u/2\pi m_0c^2$ is the undulator parameter, γ is the electron-beam relativistic factor, and $\Omega_u=2\pi c/\lambda_u$ is the frequency associated to the undulator period. (c) The electron beam, at the undulator input, is distributed in phase space as

$$W(\eta,\eta')=\frac{1}{2\pi\varepsilon_\eta}\exp\left\{-\frac{1}{2}\frac{\beta_\eta\eta'^2+2\alpha_\eta\eta\eta'+\gamma_\eta\eta^2}{\varepsilon_\eta}\right\} \qquad (\eta=x,y) \ ,$$

where $\pi\varepsilon_\eta$ is the electron beam emittance

$$\beta_\eta\gamma_\eta-\alpha_\eta^2=1 \ . \tag{2}$$

(d) The electron beam is said to be matched whenever

$$\beta_\eta^*=\frac{\gamma}{\pi K}\lambda_u=\frac{c}{\Omega_\eta} \tag{3}$$

and $\alpha_\eta=0$.

When the betatron motion is included, new harmonics due to the betatron oscillations contribute to the brightness. The analytical expression providing the brightness is significantly more intricate than the usual expression [2]. In fact, one obtains [3]

$$\frac{d^2I}{d\omega\,d\Omega}=\frac{e^2N^2}{c}\left|\sum_{\{i\}}\frac{\omega}{\Omega_u}\{(T^x_{\{i\}}+T^y_{\{i\}})\mathcal{H}_{\{i\}}\}\right|^2 , \qquad \{i\}=m,n,p,k,l \ , \tag{4}$$

where

$$\mathcal{H}_{\{i\}}=\left[\frac{\sin(\frac{1}{2}\nu_{m,n,p,k,l})}{\frac{1}{2}\nu_{m,n,p,k,l}}\right]e^{-\frac{1}{2}\nu_{m,n,p,k,l}} ,$$

$$\nu_{m,n,p,k,l}=-2\pi N\frac{\omega-m\omega_u-n\omega_x-p\omega_y-\kappa(\omega_u-\omega_x)-l(\omega_u+\omega_x)}{\omega_u} ,$$

$$\omega_r=\frac{2\gamma^2\Omega_r}{1+K^2/2+\gamma^2(H_x+H_y)} \ , \quad H_\eta=\tfrac{1}{2}[\eta'^2(0)+\beta_\eta^{*-2}\eta^2(0)], \quad \eta=x,y \ . \tag{5}$$

The symbol $\{i\}$ denotes the various harmonics. The harmonic oscillator Hamiltonian H_η specifies the betatron motion Hamiltonian, $\eta(0)$ and $\eta'(0)$ are the off-axis phase-space initial coordinates. The amplitudes $T^{(x,y)}_{\{i\}}$ are specified by

$$T^x_{\{i\}}=\left\{-\frac{K}{\gamma}[J_{(m-1)/2}(-A)+J_{(m+1)/2}(-A)]\mathcal{D}_n(B_x,C_x)\right.$$
$$\left.-\tfrac{1}{2}J_{m/2}(-A)\{[x'(0)+i\beta_x^{*-1}x(0)]\mathcal{D}_{n+1}(B_x,C_x)+[x'(0)-i\beta_x^{*-1}x(0)]\mathcal{D}_{n-1}(B_x,C_x)\}\right\}$$
$$\times\mathcal{D}_p(B_y,C_y)R_\kappa(D_-,F_-)R_l(D_+,F_+)\;;$$

$$T^y_{\{i\}}=-\frac{1}{2}\{[y'(0)+i\beta_y^{*-1}y(0)]\mathcal{D}_{p+1}(B_y,C_y)+[y'(0)-i\beta_y^{*-1}y(0)]\mathcal{D}_{p-1}(B_y,C_y)\}$$
$$\times J_{m/2}(-A)\mathcal{D}_n(B_x,C_x)R_\kappa(D_-,F_-)R_l(D_+,F_+)\;, \tag{6a}$$

where

$$A=\frac{1}{8}\left[\frac{K}{\gamma}\right]^2\frac{\omega}{\Omega_u},\quad B_\eta=i\frac{\omega}{4c}\eta(0)\eta'(0)\;,$$
$$C_\eta=-\frac{\omega}{2}\mathcal{L}_\eta(0)\;,$$
$$\mathcal{L}_\eta(0)=\frac{1}{4\Omega_\eta}\left[\eta_0'^2-\left[\frac{\Omega_\eta}{c}\eta(0)\right]^2\right],\quad \eta=x,y\;,$$
$$D_\pm=\pm\frac{iK}{2\gamma c}\omega\frac{x_1(0)\Omega_x}{\Omega_u\pm\Omega_x},\quad F_\pm=\frac{K}{2\gamma}\frac{x'(0)\omega}{\Omega_u\pm\Omega_x}\;,$$
$$\mathcal{D}_n(x,y)=\sum_{l=-\infty}^{+\infty}I_{(n-l)/2}(x)J_{l/2}(y)\;,$$
$$R_n(x,y)=\sum_{l=-\infty}^{+\infty}I_{n-l}(x)J_l(y)\;. \tag{6b}$$

If we keep $\eta(0)=\eta'(0)=0$, Eq. (4) reduces to the usual expression; the extra contributions are just due to the inclusion of the off-axis motion effects. (For further comments see Ref. [3].) The position of the peak of a given harmonic is provided by the value of ω for which the argument of the sinc in Eq. (4) vanishes. Since $\Omega_{x,y}/\omega_u \ll 1$, the most significant contribution to identifying the peak should come from the integer $m+\kappa+l$. The additional terms should contribute with a not particularly significant shift. The summations on the indices are, however, independent. One can, therefore, identify the harmonic with the index m and arrange the summations in such a way that the κ and l indices of the sine argument cancel each other. This does not mean that we are eliminating the dependence on these indices, which otherwise contribute through the Bessel functions.

The considerations we have developed refer to the case of a single electron injected into the undulator with initial phase-space coordinates (x_0,x_0',y_0,y_0'). The effect of the whole beam is obtained by averaging Eq. (4) on the phase-space distribution (2). Assuming a sinc^2 shape for the spectrum of the nth harmonic, the line distortion effects due to the electron beam phase-space distribution are evaluated performing a "naive" convolution [1] on (2), thus getting

$$F(\nu_m)=2|\mathrm{Re}\int_0^1 dt\frac{(1-t)e^{i\nu_m t}}{[R_x^{(m)}(t)R_y^{(m)}(t)]^{1/2}}\;, \tag{7}$$

where

$$R_\eta^{(m)}(t)=(1+\alpha_\eta^2)(1+i\pi m\mu_\eta t)(1+i\pi m\mu_{\eta'}t)-\alpha_\eta^2\;,$$
$$\mu_\eta=\frac{2N\gamma^2\varepsilon_\eta}{(1+K^2/2)\beta_\eta},\quad \mu_{\eta'}=\frac{2N\gamma^2}{(1+K^2/2)}\frac{1}{\beta_\eta^{*2}}\frac{\varepsilon_\eta}{\gamma_\eta}\;. \tag{8}$$

Equation (7) provides the spectrum inhomogeneous broadening and the dependence on the electron beam Twiss parameters. To give an idea of the spectrum distortion due to the various electron beam parameters, which affects the brightness, in Fig. 1 we have plotted the brightness of the first harmonic for the parameters reported in Table I(a) and for different values of the Twiss coefficients. For a matched beam, owing to the smallness of the emittances, the spectrum is almost insensitive to inhomogeneous broadening effects. When α_η, β_η, and γ_η deviate from the matching condition, the spectrum is

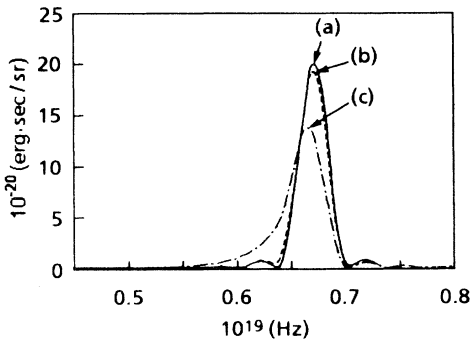

FIG. 1. First-harmonic brightness vs frequency parameters of Table I(a). Curve a: $\alpha_x=\alpha_y=0$, $\beta_x=\beta_y=\beta^*=(\gamma/\pi K)\lambda_u$. Curve b: $\alpha_x=\alpha_y=1$, $\beta_x=\beta_y=\beta^*$. Curve c: $\alpha_x=\alpha_y=0.5$, $\beta_x=\beta_y=\beta^*/10$.

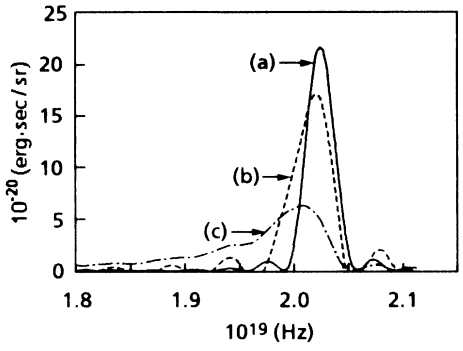

FIG. 2. Third-harmonic brightness vs frequency. Curve *a*: $\alpha_x=\alpha_y=0$, $\beta_x=\beta_y=\beta^*$; $\varepsilon_x=\varepsilon_y=0$. Curve *b*: $\alpha_x=\alpha_y=0$, $\beta_x=\beta_y=\beta^*$; emittances $\varepsilon_x=7\times10^{-7}$ (cm rad), $\varepsilon_y=8\times10^{-8}$ (cm rad). Curve *c*: $\alpha_x=\alpha_y=1$, $\beta_x=\beta_y=\beta^*/10$; emittances: same as case (b).

broadened and distorted. The reduction and distortion effects are more evident for higher harmonics. The electron beam effects on the third-harmonic brightness are shown in Fig. 2: the emittance, albeit small, produces a sizable inhomogeneous broadening even in the matched case. One of the effects of the inclusion of the off-axis motion in the analysis of undulator brightness is the presence of on-axis even harmonics.

To evaluate, e.g., the second on-axis harmonic, we are forced to perform a rather crude approximation, which is of the same type as that used to evaluate the odd harmonic case, but more doubtful, since in this case the emission is dominated by the betatron motion (see Ref. [1]).

To perform the calculation and carry out the integration on the phase-space distribution, we neglect, in Eqs. (6), all the $(\mathcal{D},R)$ functions having index larger than 0 and make the further assumption that

$$(D_0,R_0)\sim(1,1)\ . \tag{9}$$

TABLE I. Parameters used in several figures.

(a) $\gamma=1.7\times10^4$, $\varepsilon_x=7\times10^{-9}$ m rad
$\varepsilon_y=0.8\times10^{-9}$ m rad, $\lambda_u=5$ cm
$N=20$, $\kappa=1.48$

(b) $\gamma=40$, $\varepsilon_x=\frac{\pi}{40}$ mm rad,
$\varepsilon_y=\frac{\pi}{40}$ mm mrad
$N=20$, $K=\sqrt{2}$, $\lambda_u=5$ cm

(c) $\gamma=40$, $\varepsilon_x=\pi$ mm mrad, $\varepsilon_y=\pi$ mm mrad
$N=20$, $K=\sqrt{2}$, $\lambda_u=5$ cm

The arbitrariness of these assumptions is evident, and we will comment on their range of validity in the next section. However, they allow us to obtain the following expression for the $m=2$ spectrum distortion:

$$F(\nu_2)=2\,\mathrm{Re}\int_0^1 dt(1-t)e^{i\nu_2 t}\left\{\frac{\gamma_x\varepsilon_x(1+2i\pi\mu_x t)}{\{[R_x^{(2)}(t)]^3R_y^{(2)}(t)\}^{1/2}}+\frac{\gamma_y\varepsilon_y(1+2i\pi\mu_y t)}{\{[R_y^{(2)}(t)]^3R_x^{(2)}(t)\}^{1/2}}\right\}. \tag{10}$$

It is evident that the second-harmonic brightness is proportional to the beam emittance and that it should become larger when the Twiss parameter γ_η increases. This is the case as shown in Fig. 3 where the second-harmonic brightness is plotted versus the frequency for a matched and a nonmatched beam. Under the latter hypothesis, the inhomogeneous broadening contributions are beneficial in the sense that the greater the emittance the higher the brightness, and it becomes even higher if the beam is mismatched by enhancing the γ_η parameter.

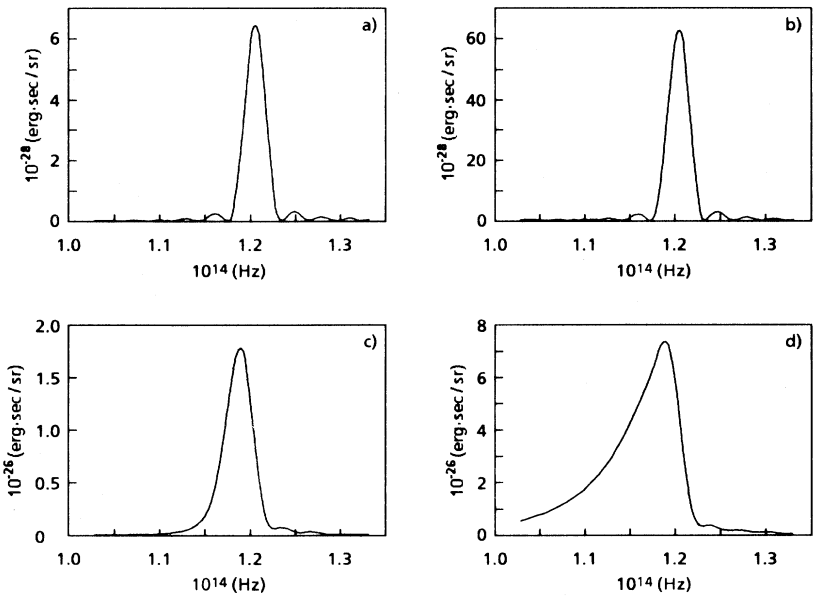

FIG. 3. (a) Second-harmonic brightness vs frequency [parameters of Table I(b)]. Matched case ($\alpha_x=\alpha_y=0$, $\beta_x=\beta_y=\beta^*$). (b) Second-harmonic brightness vs frequency [parameters of Table I(b)]. Unmatched case ($\alpha_x=\alpha_y=0$, $\beta_x=\beta_y=\beta^*/10$). (c) Second-harmonic brightness vs frequency [parameters of Table I(c)]. Matched case ($\alpha_x=\alpha_y=0$, $\beta_x=\beta_y=\beta^*$): (d) Second-harmonic brightness vs frequency [parameters of Table I(c)]. Unmatched case ($\alpha_x=\alpha_y=0$, $\beta_x=\beta_y=\beta^*/10$).

II. COMPARISON BETWEEN ANALYTICAL AND NUMERICAL RESULTS

The numerical procedure exploited to include the effect of the initial electron beam phase-space distribution is based on a Monte Carlo sampling of the mean electron brightness as a function of the frequency. The initial values x_0, y_0, x_0', y_0' of each electron trajectory are obtained, using a Neumann procedure [4], from the distribution function (2). Recalling that the brightness, namely, the energy radiated per unit solid angle and unit frequency intervals, is given by the well-known expression [5] ($s=\beta ct$)

$$\frac{d^2I}{d\Omega\, d\omega}=\frac{e^2\omega^2}{4\pi^2c^3}\left|\int_{-\infty}^{+\infty}[\mathbf{n}\times(\mathbf{n}\times\boldsymbol{\beta})]\exp\left[i\frac{\omega}{c}(s-\mathbf{n}\cdot\mathbf{r})\right]ds\right|^2, \tag{11}$$

where $\mathbf{n}$ is a unit vector determining the direction of observation, and $\mathbf{r}$ and $\boldsymbol{\beta}$ specify the particle position and velocity, respectively, we treat the problem numerically, solving the system of ordinary differential equations ($\alpha=x,y,z$):

$$\frac{d}{ds}f_\alpha^R=[\mathbf{n}\times(\mathbf{n}\times\boldsymbol{\beta})]_\alpha\cos\left[\frac{\omega}{c}(s-\mathbf{n}\cdot\mathbf{r})\right];\quad \frac{d}{ds}f_\alpha^I=[\mathbf{n}\times(\mathbf{n}\times\boldsymbol{\beta})]_\alpha\sin\left[\frac{\omega}{c}(\mathbf{s}-\mathbf{n}\cdot\mathbf{r})\right];$$

$$\frac{d^2}{ds^2}x=\left[\frac{2\pi}{\lambda_u}\right]\frac{K}{\gamma}\left[A(x,y)\frac{dz}{ds}\sin\left[2\pi\frac{z}{\lambda_u}\right]-\kappa_u y(s)\frac{dy}{ds}\cos\left[2\pi\frac{z}{\lambda_u}\right]\right];$$

$$\frac{d^2}{ds^2}y=\left[\frac{2\pi}{\lambda_u}\right]\frac{K}{\gamma}\left[\frac{dx}{ds}\cos\left[2\pi\frac{z}{\lambda_u}\right]-\frac{\kappa_u}{2}\delta x(s)\frac{dz}{ds}\sin\left[2\pi\frac{z}{\lambda_u}\right]\right]y(s);$$

$$\frac{d^2z}{ds^2}=\left[\frac{2\pi}{\lambda_u}\right]\frac{K}{\gamma}\left[\frac{1}{2}\left[\frac{2\pi}{\lambda_u}\right]^2\delta x(s)y(s)\frac{d}{ds}y(s)-A(x,y)\frac{dx}{ds}\right]\sin\left[2\pi\frac{z}{\lambda_u}\right]; \tag{12}$$

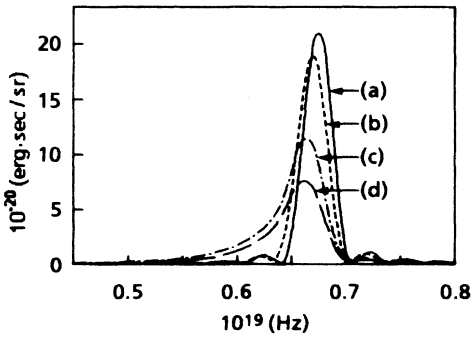

FIG. 4. First-harmonic brightness vs frequency [parameters of Table I(a)]. Curve *a*: Analytical approximation; curve *b*: numerical analysis, $\alpha_x=\alpha_y=0$, $\beta_x=\beta_y=\beta^*$; curve *c*: analytical approximation; curve *d*: numerical analysis, $\alpha_x=\alpha_y=1$, $\beta_x=\beta_y=\beta^*/10$.

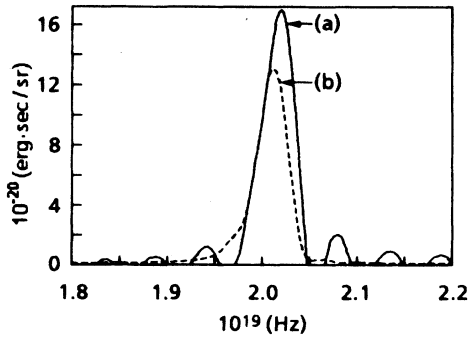

FIG. 5. Third-harmonic brightness vs frequency [parameters of Table I(a)]. Curve *a*: Analytical approximation; curve *b*: numerical analysis, $\alpha_x=\alpha_y=0$, $\beta_x=\beta_y=\beta^*$.

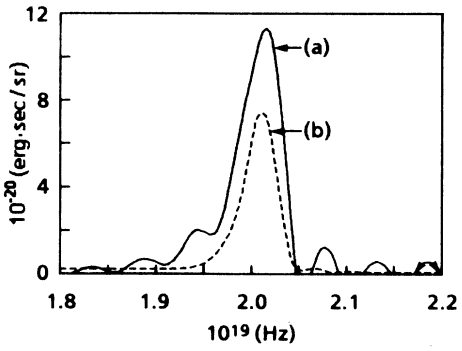

FIG. 6. Same as Fig. 5. $\alpha_x=\alpha_y=0.5, \beta_x=\beta_y=\beta^*/5$.

where

$$A(x,y)=1+\frac{1}{4}\left[\frac{2\pi}{\lambda_u}\right]^2[\delta x^2(s)+(2-\delta)y^2(s)] . \quad (13)$$

The last three equations in (12) are the Lorentz force equation for an electron moving in a magnetic field with components

$$B_x(x,y,z)=\tfrac{1}{2}B_0\delta\kappa_u^2 xy\sin(\kappa_u z) ,$$

$$B_y(x,y,z)=B_0\left\{1+\tfrac{1}{4}\kappa_u^2[\delta x^2+(2-\delta)y^2]\sin(\kappa_u z)\right\} ,$$

$$B_z(x,y,z)\cong B_0\kappa_u y\cos(\kappa_u z) ,$$

$$\kappa_u=2\pi/\lambda_u . \quad (14)$$

The magnetic field has been expanded up to the lowest order in the transverse coordinates (x,y) [6]. We choose $\delta=1$ so as to have a magnet focusing equally in both radial and vertical directions.

The initial conditions of the system (12) are specified by

$$x(0)=x_0, \quad \left.\frac{dx}{ds}\right|_{s=0}=x_0'-\frac{K}{\gamma} ;$$

$$y(0)=y_0, \quad \left.\frac{dy}{ds}\right|_{s=0}=y_0' ;$$

$$z(0)=0, \quad \left.\frac{dz}{ds}\right|_{s=0}=(\beta^2-x_0'^2-y_0'^2)^{1/2} . \quad (15)$$

The solution is evaluated in the interval $[0,L_u]$ $(L_u=N\lambda_u)$ and the brightness is expressed as

$$\frac{d^2I}{d\omega\, d\Omega}=\frac{e^2}{4\pi^2 c}\left[\frac{\omega}{c}\right]^2\sum_\alpha\{[f_\alpha^R(L_u)-f_\alpha^R(0)]^2+[f_\alpha^I(L_u)-f_\alpha^I(0)]^2\} . \quad (16)$$

The results of the integration are shown in Figs. 4–6, where we make a comparison with the results from the analytical treatment. In the figures we show the prediction of the first- and third-harmonic brightness for matched and nonmatched cases. It is evident that when we move away from the matching condition, the two methods provide results whose difference becomes more significant.

Even for the matched case, where substantial agreement exists between the two methods, the difference becomes more evident with increasing order of harmonic.

Figure 7 and 8 show the first- and third-harmonic brightness for the parameters of Table I(b) and I(c). It is

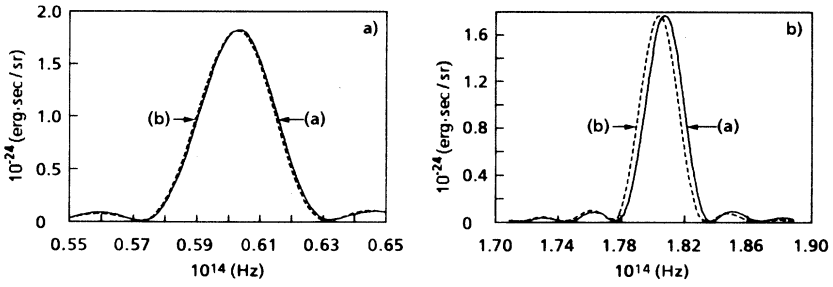

FIG. 7. (a) First-harmonic brightness vs frequency [parameters of Table I(b)]. Curve *a*: Analytical approximation; curve *b*: numerical analysis, matched case $(\alpha_x=\alpha_y=0, \beta_x=\beta_y=\beta^*)$. (b) Third-harmonic brightness vs frequency. Same as (a).

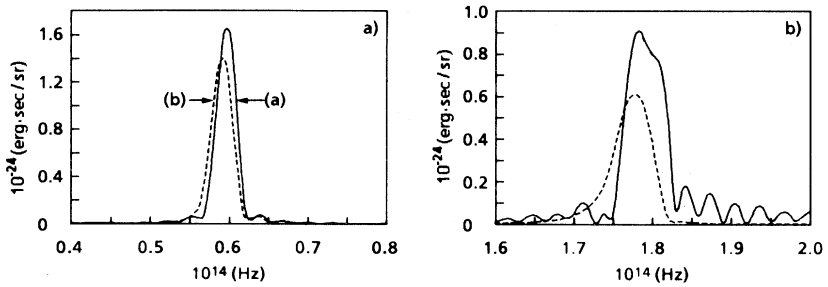

FIG. 8. (a) First-harmonic brightness vs frequency [parameters of Table I(c)]. Same as Fig. 7(a). (b) Third-harmonic brightness vs frequency [parameters of Table I(c)]. Same as Fig. 7(a).

evident that the agreement between the analytical and the numerical analysis becomes less satisfactory with increasing emittance. As expected, the analytical approximation totally fails in predicting the amplitude of the second harmonic (see Figs. 9 and 10).

The problem now is to understand the reason for the discrepancies. We recall that, to perform the average on the distribution (2), we neglected the D and R functions with indices whose modulus is greater than 0 and we made the further assumption (14). We will see why this approximation may not work. The use of the Graf addition theorem [7] lets us write

$$R_0(x,y)=J_0\sqrt{x^2+y^2} \tag{17}$$

and for our variables[1]

$$R_0(D_\pm,F_\pm)\cong J_0\left[\frac{\gamma K}{1+K^2/2}\sqrt{x_0'^2+(\Omega_x^2 x_0)^2}\right]. \tag{18}$$

Expanding the Bessel function up to the lowest order and integrating over the phase-space distribution, we find[2]

$$\langle R_0(D_\pm,F\pm)\rangle\cong 1-\frac{1}{8N}\frac{K}{1+K^2/2}(1+\alpha_x^2)(\mu_x+\mu_{x'}) . \tag{19}$$

The correcting term may be negligible if the beam is matched and, thus, the inhomogeneous broadening contributions are minimized; otherwise, the mismatching may cause a sensible correction.

The modulating function due to the betatron motion may induce corrections. Proceedings as in the previous case, we write

$$\mathcal{D}_0(B_\eta,C_\eta)=J_0(\sqrt{B_\eta^2+C_\eta^2})\cong\left[1-\frac{1}{4}\left\{\frac{\gamma^4(2\pi)^2}{4\lambda_u^2(1+K^2/2)^2}(\eta_0\eta_0')^2+\frac{\gamma^6}{4}\frac{1}{K^2(1+K^2/2)^2}\left[\eta_0'^2-\left[\frac{\Omega_\eta}{c}\eta_0\right]^2\right]^2\right\}\right] . \tag{20}$$

Averaging on the initial phase-space distribution, we find that the second term in the curly brackets vanishes for a matched beam, while the first term can be neglected if

$$\pi\varepsilon_\eta\ll\lambda=\frac{\lambda_u}{2\gamma^2}(1+K^2/2) . \tag{21}$$

It is clear that, when the matched condition or the inequality (21) does not hold, $\mathcal{D}_0$ cannot be approximated with 1.

The reason for the discrepancy between analytical and numerical results may, however, derive from other facts. Most of the examples discussed so far refer to an electron beam with very large energy ($\gamma\cong 1.4\times 10^4$), so the betatron wavelength is much larger than the undulator length itself. This means that the representation of the betatron motion in terms of trigonometric functions, even though

[1]We have substituted ω with $2\gamma^2\omega_u/(1+K^2/2)$ and neglected $\Omega_{x,y}$ with respect to Ω_u.

[2]Where the brackets denote an average on the phase-space distribution.

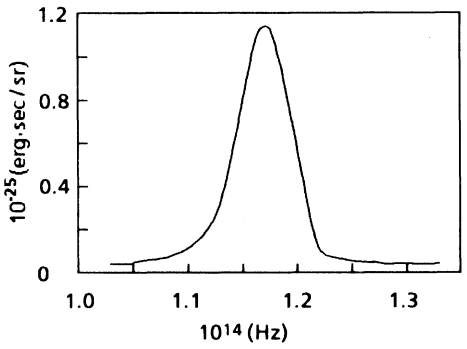

FIG. 9. Second-harmonic brightness vs frequency. Numerical analysis. Same parameters as Fig. 3(c). Analytical and numerical predictions differ by about one order of magnitude.

correct from the analytical point of view, may be doubtful for computational purposes. In addition, the concept itself of betatron harmonics may sound rather artificial. This interpretation is supported by the result of Fig. 11, where we have compared the results relative to the independent methods: (a) numerical integration of the electron trajectory and of the Lienard-Wiechert integral; (b) numerical integration of the Lienard-Wiechert integral using the analytical approximation of the electron trajectory; (c) fully analytical computation, i.e., use of Eq. (4) fixing the phase-space initial coordinates (x_0, x_0', y_0, y_0').

It is evident that (b) and (c) yield almost equivalent results, which differ substantially from method (a) in the case of large γ. Furthermore, when γ is large, a reasonable convergence of the brightness is provided by including a large number of contributions from the indices n and p as indicated in Fig. 12. A further delicate point comes from the relative error required in the computation of Bessel functions when a large number of contributions from $\mathcal{D}$ modulation is included. The different predictions requiring relative errors of 10^{-6} and 10^{-8} are shown in Fig. 13.

It is evident that the analytical approximations of Sec. II are hampered by the crude assumption that the various modulating terms can be approximated with 1. Such an approximation becomes unsatisfactory for harmonics dominated by betatron motion, as in the case of even on-axis harmonics. However, it should be understood that Eq. (4), providing the single-electron brightness, without the average on the phase-space distribution is in close agreement with the numerical calculation performed using the analytical approximation of the electron motion. Furthermore, some differences appear for the case of full numerical integration when the phase-space coordinates are taken far from the center of the distribution (see Fig. 14). Even though Eq. (4) allows one to understand the interplay between the various motion components in the emission process, its convolution on the distribution (2) can be achieved only with great difficulty and, therefore, a numerical integration appears unavoidable. However, all the numerical procedures necessary to check the relia-

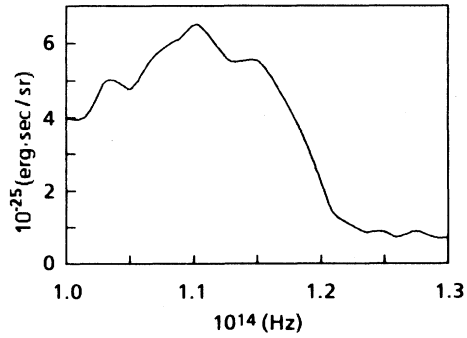

FIG. 10. Second-harmonic brightness vs frequency. Same as Fig. 9. Nonmatched case ($\alpha_x = \alpha_y = 0, \beta_x = \beta_y = \beta^*/10$).

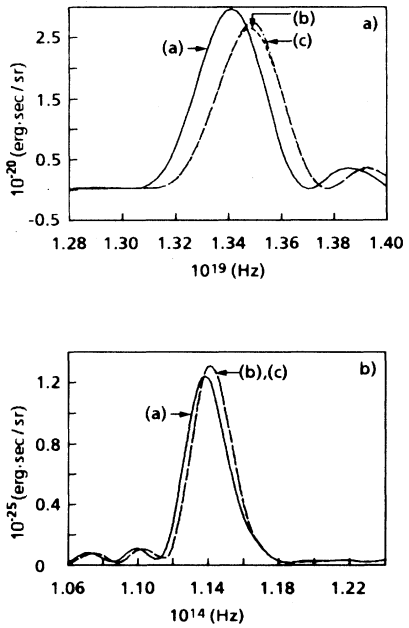

FIG. 11. (a) Second-harmonic brightness vs frequency [Table I(a)]. Curve *a*: Fully numerical analysis; curve *b*: analytical approximation of the electron trajectory and numerical integration of the Lienard-Wiechert integral; curve *c*: Bessel function expansion [Eq. (5)] $x_0 = 1 \times 10^{-1}$ cm, $y_0 = 3 \times 10^{-2}$ cm, $x_0' = 6.8 \times 10^{-6}$ cm, $y_0' = 2 \times 10^{-6}$ cm. The last result has been obtained by keeping the contribution on the n index between -200 and $+200$. The plot refers to the "single-electron" case and does not contain integration on the phase-space distribution. (b) Same as (a) (parameters $K = 1.48$, $\gamma = 40$, $N = 20$). The *b* and *c* computations are indistinguishable.

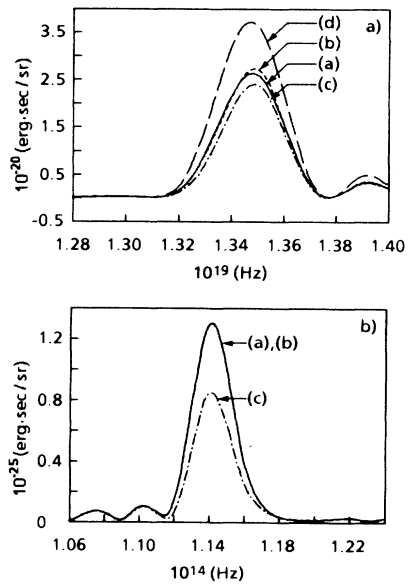

FIG. 12. (a) Second-harmonic brightness vs frequency ($\gamma=1.4\times10^4$). Curve *a*: Analytical approximation of the electron trajectory and numerical integration of the Lienard-Wiechert integral; curve *b*: Same as *c* in Fig. 11(a); curve *c*: Same as *b* but with *n* ranging from -100 to 100; curve *d*: Same as *b* but with *n* ranging from -28 to 28. (b) Same as (a) ($\gamma=40$). Curve *a*: Bessel function expansion $n=-4,4$; curve *b*: Same as *a* $n=-2,2$; curve *c*: Same as *a* $n=0$.

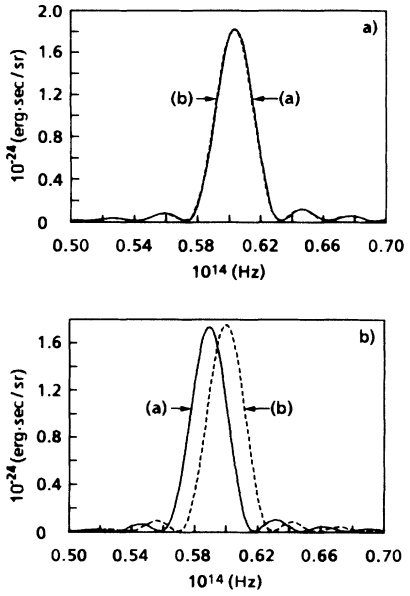

FIG. 14. (a) First-harmonic brightness vs frequency. Curve *a*: analytical procedure. Curve *b*: numerical procedure [parameters of Table I(b) $x_0=y_0=x_0'=y_0'=0$]. (b) Same as (a). Curve *a*: Full numerical computation; curve *b*: analytical computation indistinguishable from the numerical integration of the Lienard-Wiechert integral using the analytical approximation of the trajectory.

bility of the computation require computer times comparable to or even longer than the fully numerical procedure.

Before concluding it is, perhaps, worth adding a few comments on the numerical computation of the generalized Bessel functions $J_n(x,y)$ and $\mathcal{D}_\xi(x,y;z,u)(\xi=n,p,\kappa,l)$, which have been calculated using the integral representatives

$$J_m(x,y)=\frac{1}{\pi}\int_0^\pi \cos(m\theta-x\sin\theta-y\sin2\theta)d\theta\ ,$$

$$|\mathrm{Re}\mathcal{D}_\xi(x,y;z,u)=\frac{1}{\pi}\int_0^\pi \cos(x\cos\theta+y\cos2\theta)\times\cos(\xi\theta-z\sin\theta-u\sin2\theta)d\theta\ ,$$

$$|\mathrm{Im}\mathcal{D}_\xi(x,y;z,u)=\frac{1}{\pi}\int_0^\pi \sin(x\cos\theta+y\cos2\theta)\times\cos(\xi\theta-z\sin2\theta)d\theta\ . \quad (22)$$

The convergence of the expansion was controlled using the Parseval condition, in the present case provided by

$$\sum_{m=-\infty}^{+\infty} J_m^2(x,y)=1,\quad \sum_{\xi=-\infty}^{+\infty}|\mathcal{D}_\xi(x,y;z,u)|^2=1\ . \quad (23)$$

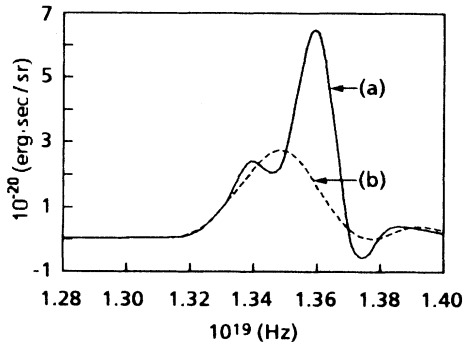

FIG. 13. Second-harmonic brightness vs frequency. Same as Fig. 12(a). Evaluation with Bessel function expansion. Curve *a*: Relative error on Bessel functions 10^{-6}; curve *b*: relative error on Bessel functions 10^{-8}.

The "messages" contained in this paper can be finally summarized below. (a) The role played by the Twiss parameters in the analysis of undulator radiation is not secondary; a possible mismatch of the electron beam may, indeed, strongly affect the brightness. (b) The inclusion of inhomogeneous broadening effects using the "naive convolution method" of Sec. II is more reliable in the case of matched beam and for the fundamental har-

monic. (c) Even in the case of matched conditions, neglecting betatron motion may give rise to substantial deviations from the correct analysis. (d) The naive method for the study of even on-axis harmonics is highly doubtful and, in this case, the numerical analysis seems to be mandatory. We will see the consequences of the present analysis on free-electron-laser dynamics in a forthcoming paper.

[1] F. Ciocci, G. Dattoli, and A. Torre, IEEE J. Quantum Electron. **30**, 793 (1994).

[2] D. F. Alferov, Yu. A. Bashmakov, and E. G. Bessonov, Proc. P. N. Lebedev Phys. Inst. (Acad. Sci. USSR) **80**, 97 (1976); B. M. Kincaid, J. Appl. Phys. **48**, 2684 (1977); W. B. Colson, IEEE J. Quantum Electron. **QE-17**, 1417 (1981); R. Barbini, F. Ciocci, G. Dattoli, and L. Giannessi, Riv. Nuovo Cimento **6** (1990).

[3] G. Dattoli, I. Giannessi, L. Mezi, M. Richetta, and A. Torre, Phys. Rev. A **45**, 4023 (1992).

[4] F. M. Sobel, *The Numerical Method Monte Carlo* (Nauka, Moscow, 1975).

[5] J. D. Jackson, *Classical Electrodynamics* (Wiley, New York, 1975), p. 677.

[6] J. P. Blewett and R. Chasman, J. Appl. Phys. **87**, 33 (1977).

[7] N. N. Watson, *A. Treatise on Bessel Functions* (Cambridge University Press, Cambridge, 1967).